Interface atomic structures and magnetic anisotropy of Fe and Pd/Fe monatomic films on Pd(001)

Tetsuro Ueno,[1,*] Masahiro Sawada,[1] Kazuhito Furumoto,[2] Tetsuro Tagashira,[2] Satoshi Tohoda,[2] Akio Kimura,[2] Shinya Haraguchi,[3] Masahito Tsujikawa,[4] Tatsuki Oda,[3,5] Hirofumi Namatame,[1] and Masaki Taniguchi[1,2]

[1]*Hiroshima Synchrotron Radiation Center, Hiroshima University, 2-313 Kagamiyama, Higashi-Hiroshima 739-0046, Japan*

[2]*Graduate School of Science, Hiroshima University, 1-3-1 Kagamiyama, Higashi-Hiroshima 739-8526, Japan*

[3]*Graduate School of Natural Science and Technology, Kanazawa University, Kanazawa 920-1192, Japan*

[4]*Center for Spintronics Integrated Systems, Tohoku University, 2-1-1 Katahira, Aoba, Sendai 980-8577, Japan*

[5]*Institute of Science and Engineering, Kanazawa University, Kanazawa 920-1192, Japan*

(Received 15 April 2012; published 11 June 2012)

The magnetic anisotropy of monatomic Fe films on Pd(001) with or without a Pd overlayer was investigated from the standpoint of interface atomic structures. Quantitative analysis included low-energy electron diffraction and x-ray magnetic circular dichroism (XMCD) experiments, and first-principles calculations were also performed on monatomic Fe and Pd/Fe systems. It was revealed that Fe atoms intermix with the Pd substrate at room temperature. A spin reorientation transition occurs at a critical Fe thickness of 1.2 monolayers (ML) in Fe/Pd(001), while in-plane magnetic anisotropy is persistent in Pd/Fe/Pd(001) throughout the entire sample. The Fe 3*d* spin and orbital magnetic moments for both systems are strongly enhanced near 1 ML Fe thickness, as compared to those of the bulk iron crystal. In addition, an induced magnetic moment in interfacial Pd atoms was observed by XMCD at the Pd $M_{2,3}$ core absorption edges. It was concluded that the $L1_0$-like tetragonally distorted interface atomic structure in monatomic Fe/Pd(001) induces the perpendicular magnetic anisotropy.

DOI: 10.1103/PhysRevB.85.224406 PACS number(s): 75.30.Gw, 75.70.−i, 61.05.jh, 31.15.A−

I. INTRODUCTION

Magnetic thin films and multilayers have been studied intensively over the past few decades because of their possibly wide applications in high-performance electronic devices exploiting the spin degrees of freedom.[1,2] In practical applications, perpendicular magnetic anisotropy (PMA)[3] and giant magnetoresistance[4,5] are the key operational principles for ultra-high-density magnetic storage devices. From a basic science standpoint, they are suitable for studying the peculiar magnetic properties driven by a reduced dimensionality, such as the reduction of Curie temperature and an enhanced magnetic moment with a lower number of coordinates. As a guideline for future magnetic material design, the underlying mechanism of these magnetic properties needs to be unveiled.

Among several magnetic multilayer systems, Pt/Fe monatomic film is known to exhibit a strong PMA.[6,7] In order to reveal the relationship between the magnetic anisotropy and electronic structures of ultrathin magnetic films, a systematic study of various combinations of 3*d* ferromagnetic elements and nonmagnetic substrate is necessary. Palladium is a 4*d* paramagnetic element on the verge of ferromagnetism because of its high density of states right at the Fermi energy.[8] Fe-Pd alloys, thin films, and multilayer systems have been studied for decades because of their fascinating magnetic properties. In particular, an FePd ordered alloy with an $L1_0$ structure exhibits uniaxial magnetic anisotropy.[9,10] Fe-Pd systems are expected to be potential candidates for compounds whose magnetic anisotropy can be manipulated using an electric field because of their relatively low magnetic anisotropy energy, as compared to others such as Fe-Pt systems. Recent experimental[11] and theoretical[12] results indicate the large electric-field effect in Fe-Pd systems.

To date, several experimental and theoretical studies have been conducted for Fe monatomic films on Pd(001). However, the growth mode and interfacial atomic structure of the system, which could be responsible for its peculiar magnetism, are still controversial. The reported results are diverse, for instance with respect to the growth mode, from island formation[13] to layer-by-layer growth.[14] There are also controversial results regarding Fe-Pd alloy formation at the interface when the films are grown at room temperature (RT).[15–17] Meyerheim *et al*. attributed the varying Fe-Pd alloy formation results to a slight difference in the substrate temperature during Fe deposition.[17] Surface magneto-optical Kerr effect (SMOKE) measurements by Liu and Bader showed a PMA for Fe films with a thickness below 2.5 monolayers (ML) grown at 100 K, while in-plane magnetic anisotropy appears below 3 ML at 300 K.[18,19] The appearance of PMA was attributed to the formation of a smooth Fe/Pd interface without intermixing for growth at low temperature. Several x-ray magnetic circular dichroism (XMCD) experiments for Fe/Pd films and multilayers have also been reported.[20–23] Le Cann *et al*. reported a constant Fe 3*d* spin magnetic moment in a wide thickness range from a few ML to 40 ML and an enhanced Fe 3*d* orbital magnetic moment with decreasing Fe film thickness.

To get a unified picture, the magnetic properties of the submonolayer or monolayer regime of Fe films need to be clarified. A quantitative determination of the magnetic moments of submonolayer and monolayer Fe on Pd(001) as well as Pd-capped Fe films is worth performing. A monatomic Pd/Fe bilayer is the thinnest limit of the $L1_0$ structure and it could be regarded as a novel PMA material with the thinnest thickness. We previously reported that a spin reorientation transition (SRT) occurs from the perpendicular to the in-plane direction with increasing Fe thickness for Fe/Pd(001), while no such SRT occurs for 1 ML Pd-capped Fe/Pd(001); however, the microscopic origin of the magnetic anisotropy remained unsolved.[24]

In this paper, detailed experimental and theoretical studies of interface atomic structures, magnetic anisotropy, and electronic structures of Fe and Pd/Fe monatomic films on

Pd(001) are presented. In order to analyze the interface atomic structures, quantitative low-energy electron diffraction analysis (LEED I-V) was carried out. To clarify the magnetic anisotropy, XMCD spectroscopy experiments were performed. XMCD spectroscopy provides useful information on the magnetic properties in an element-specific way. In addition, first-principles calculations were carried out to study the magnetic anisotropy and electronic structures of Fe and Pd/Fe monatomic films.

II. METHODS

A. Sample fabrication

The Pd(001) single crystalline substrate (10 mm in diameter) was cleaned by repeated cycles of Ar^+ bombardment at 1 kV and annealing at 973 K for 10 min in ultra-high vacuum (UHV). Prior to the film growth, Auger electron spectroscopy (AES) was performed to confirm negligible amounts of contaminants. Fe and Pd were deposited onto the substrate at RT (310 K) via an e-beam evaporation source. The deposition rates of Fe and Pd were 0.3 and 0.2 ML/min, respectively, which were calibrated using the specular spot intensity oscillations in reflection high-energy electron diffraction (RHEED) measurements. Clear RHEED oscillation was observed for both Fe deposition on Pd(001) and Pd deposition on Fe/Pd(001), which confirms the layer-by-layer growth. Film thickness was cross-checked by the intensity ratio of Fe *LMM* (651 eV) with respect to Pd *MNN* (330 eV) in the AES spectra. In order to study the thickness dependence of the magnetic properties and magnetic moments, a wedge-shaped film was prepared for XMCD experiments. Homogeneously deposited films were also used for the LEED I-V experiment. All of the experiments were performed under UHV conditions in order to avoid surface contamination and oxidation.

B. LEED I-V experiment

For the LEED I-V measurements, the incident electron beam energy was scanned from 50 to 400 eV in 2 eV steps. The intensities of two inequivalent beams [(10) and (11)] were extracted, and the total energy range (E_T) considered was 590 eV. The experimental I-V curves were normalized using the incident electron beam current, and the intensities of symmetrically equivalent beams were averaged. The LEED I-V calculation was performed using the Barbieri/Van Hove SATLEED package.[25] The angular momentum of the phase shift of Fe and Pd was considered up to 12 and the thermal effect was included. Pendry's R factor (R_P) was employed to estimate the reliability of the calculated I-V curves.[26] The error of R_P (δR_P) is defined as $\delta R_P = R_P\sqrt{8|V_{0i}|/E_T}$, where V_{0i} is the imaginary part of the inner potential. The initial value of V_{0i} was set to -4 eV, which is a typical value for LEED I-V calculation. The error of the interlayer distance (δd) was defined as the distance variation in the range of δR_P.

The averaged T-matrix approximation (ATA) was adopted for taking into account a possible intermixing between Fe and Pd atoms at the interface. ATA is generally used for randomly mixed systems such as the disordered alloy, where the pseudoelement atoms are assumed for the alloying.[27,28] The scattering T matrix of the pseudoelement is given as the weighted average of the T matrices of several elements present. The structural models used in the calculation are shown in Fig. 1. The in-plane lattice constant (d_a) was set to be the same as that of fcc Pd (2.75 Å). The averaged T-matrix element of the pseudoelement is defined as shown in Eq. (1):

$$t^n_{\text{pseudo}} = C^n_{\text{Fe}} t_{\text{Fe}} + \left(1 - C^n_{\text{Fe}}\right) t_{\text{Pd}}, \tag{1}$$

where t^n_{pseudo}, t_{Fe}, and t_{Pd} are the T-matrix elements of the pseudoelement in the nth, Fe, and Pd layers, respectively, and C^n_{Fe} ($0 \leqslant C^n_{\text{Fe}} \leqslant 1$) is the iron composition of the nth layer. The atomic mass and Debye temperature (470 K for Fe and 274 K for Pd) are also averaged with the same weights as shown in Eq. (1).

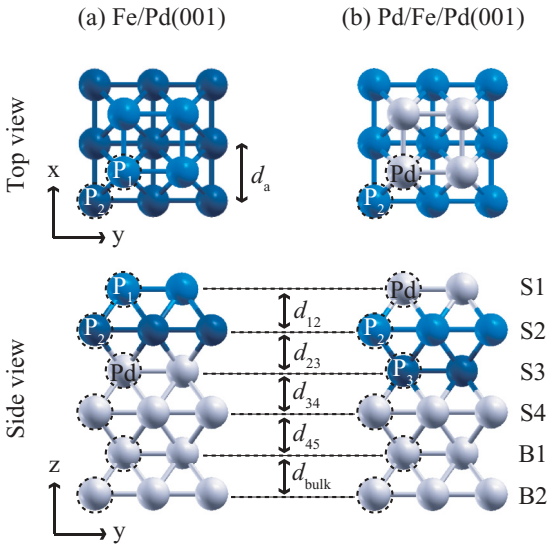

FIG. 1. (Color online) Structural models of (a) 1 ML Fe/Pd(001) and (b) 1 ML Pd/1 ML Fe/Pd(001) used in the LEED I-V calculation with the averaged T-matrix approximation. Gray (bright) balls represent the Pd atoms. Blue (dark) balls represent the pseudoelement atoms P_1, P_2, and P_3 in the layers S1, S2, and S3. The dashed circles represent the atoms in the unit cell in the calculation. Layers S1, S2, S3, and S4 are displaced along the z direction to optimize the lattice parameters (d_{12}, d_{23}, d_{34}, d_{45}). Two bulk layers B1 and B2 are fixed to maintain d_{bulk} = 1.945 Å (layer distance along the [001] direction of fcc Pd). The in-plane lattice constant d_a = 2.75 Å (nearest-neighbor distance) is also set to the same value as that in fcc Pd.

C. XAS and XMCD experiments

X-ray absorption spectroscopy (XAS) and XMCD experiments were performed at HiSOR-BL14 of Hiroshima Synchrotron Radiation Center (HSRC), Hiroshima University.[29,30] XAS spectra were acquired via the total electron yield method by measuring the sample drain current. During the XMCD experiment, the sample was cooled using liquid N_2 and the base pressure was below 5.0×10^{-8} Pa. The sample was magnetized using either (i) a pulsed magnetic field (Helmholtz coil, 0.2 T), (ii) the electromagnet (EM, 0.3 T), or (iii) the permanent magnet (PM, 1.3 T). The Helmholtz coil, EM, and PM were used in the XMCD experiment for the remanent magnetization, M-H curve measurement, and quantitative analysis of magnetic moments, respectively. The degree of circular polarization (P_c) of the incident photon was 0.8 in the

Fe $L_{2,3}$ core absorption region. For all the XMCD experiments conducted here, the sample magnetization direction was switched, while the incident photon helicity was fixed, in order to observe the dichroic signal. In the XMCD experiments using the PM, the magnetic field was switched parallel and antiparallel to the photon helicity at each photon energy. The element-specific *M-H* (ESMH) curves were obtained by measuring the sample drain current at the Fe L_3 edge.

D. First-principles calculation

The present first-principles calculation is based on the generalized gradient approximation[31] in Kohn-Sham theory.[32] The fully relativistic pseudopotential approach developed previously was employed.[33] The wave functions demonstrate two-component spinor form[34] and are determined self-consistently with the effect of spin-orbit interaction (SOI) embedded in the pseudopotential,[35] which is the primary origin of magnetic anisotropy. Energy cutoffs of 30 and 300 Ry were taken for the wave functions and densities, respectively.[36] For surface relaxations, atomic forces deduced from the wave functions were used, including the SOI effect. The magnetic anisotropy energy (MAE) derived from the SOI (E_{SO}) was estimated to be the difference between the total energies defined by E_{lmn} when the system is magnetized along the [lmn] direction. Thus E_{SO} can be defined as $E_{SO} = E_{100} - E_{001}$. The contribution of MAE from the magnetic dipole-dipole interaction (E_D) was also considered.[37] In the self-consistent electronic structure calculations, a $30 \times 30 \times 1$ mesh was used in k-point sampling.[38] All of the MAEs are estimated using a fixed atomic configuration for the relaxed surface systems. The spin and orbital magnetic moments on the atoms (m_{spin} and m_{orb}, respectively) were estimated within a sphere of radius of 1.32 Å for both Fe and Pd atoms.

The MAE values were calculated for 1 ML Fe/Pd(001), 2 ML Fe/Pd(001), 1 ML Pd/1 ML Fe/Pd(001), and 2 ML Pd/1 ML Fe/Pd(001). The substrate has a (001) surface typical of fcc Pd ($a_{fcc} = 3.89$ Å) comprised of five MLs in the present model systems. It was assumed that the Fe atoms sit on all of the fourfold hollow sites of Pd(001) and that the Pd atoms are placed at the hollow sites of the Fe layer. The unit cell contains six (Fe, 5 Pd), seven (2 Fe, 5 Pd; or Fe, 6 Pd), or eight (Fe, 7 Pd) atoms for 1 ML Fe/Pd(001), 2 ML Fe/Pd(001), 1 ML Pd/1 ML Fe/Pd(001), and 2 ML Pd/1 ML Fe/Pd(001) systems, respectively. The atomic coordinates of the surface were relaxed except for the three bottom layers of the substrate. A vacuum layer about 11.4 Å thick is assumed in these slab models.

III. RESULTS AND DISCUSSION

A. Interface atomic structures

In order to elucidate the interface atomic structures of Fe and Pd/Fe films on Pd(001), LEED *I-V* experiments were performed. Figure 2 shows the LEED patterns of Pd(001), Fe/Pd(001), and Pd/Fe/Pd(001) measured at RT. Spots for (10) and (11) are indicated by the dashed circles in Fig. 2(a). The LEED pattern of a Pd(001) clean surface shows sharp $p(1\times1)$ spots [Fig. 2(a)], and no extra spots are observed. After Fe deposition, these spots become diffuse with a higher background intensity, while the $p(1\times1)$ periodicity

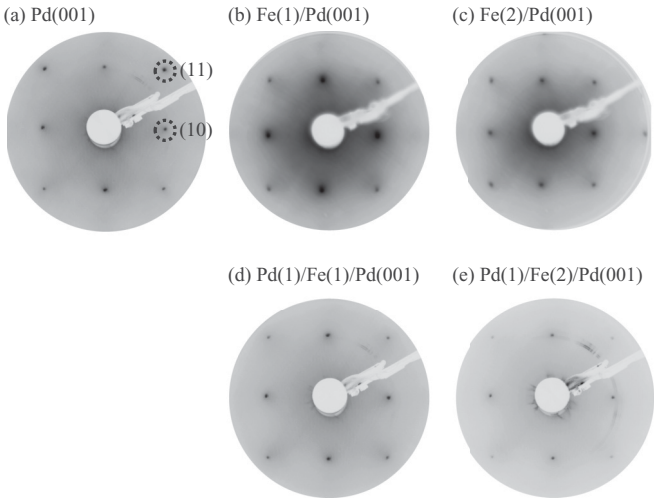

FIG. 2. (Color online) LEED patterns of (a) Pd(001) clean surface, (b) 1 ML Fe/Pd(001), (c) 2 ML Fe/Pd(001), (d) 1 ML Pd/1 ML Fe/Pd(001), and (e) 1 ML Pd/2 ML Fe/Pd(001). The LEED patterns were acquired with a primary electron energy of 130 eV at room temperature. The (10) and (11) spots are indicated by dashed circles in (a).

persists [Figs. 2(b) and 2(c)]. The spots become sharp again, maintaining the $p(1\times1)$ periodicity, after 1 ML Pd is deposited on the Fe-coated surface [Figs. 2(d) and 2(e)].

First, the interface atomic structure of the Fe-coated surface was investigated to see whether intermixing occurs. In Fig. 3(a), the experimental LEED *I-V* curves for the

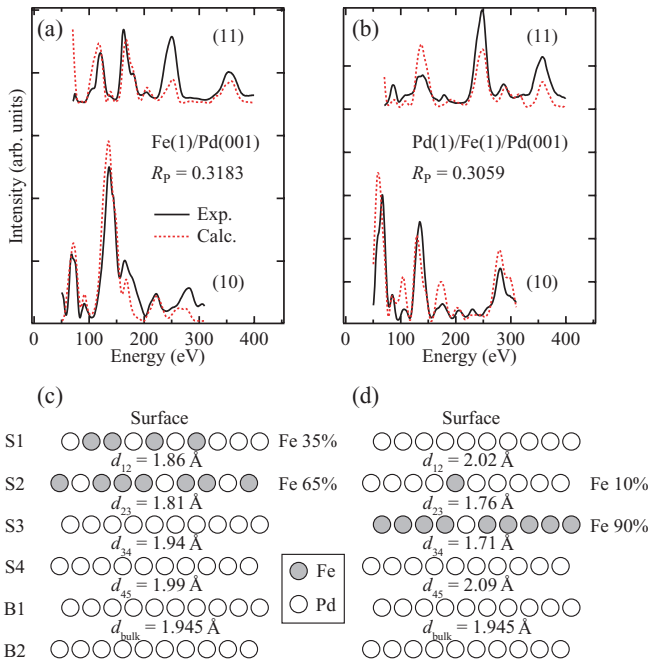

FIG. 3. (Color online) LEED *I-V* curves for the (10) and (11) spots of (a) 1 ML Fe/Pd(001) and (b) 1 ML Pd/1 ML Fe/Pd(001) measured at room temperature. Solid and dashed lines indicate experimentally and theoretically obtained curves, respectively. Optimized surface atomic structures for (c) 1 ML Fe/Pd(001) and (d) 1 ML Pd/1 ML Fe/Pd(001) are shown in the lower panel. Gray and white balls denote Fe and Pd atoms, respectively.

TABLE I. Relative interlayer relaxation $\Delta d_{ij}/d_{\text{bulk}}$ and Fe composition C^1_{Fe}, C^2_{Fe}, and C^3_{Fe} for 1 ML Fe/Pd(001) and 1 ML Pd/1 ML Fe/Pd(001) determined by LEED I-V experiments as shown in Figs. 3(c) and 3(d).

	Fe/Pd(001)	Pd/Fe/Pd(001)
$\Delta d_{12}/d_{\text{bulk}}$	−4.3%	3.9%
$\Delta d_{23}/d_{\text{bulk}}$	−6.9%	−9.5%
$\Delta d_{34}/d_{\text{bulk}}$	−0.3%	−12.1%
$\Delta d_{45}/d_{\text{bulk}}$	2.3%	7.5%
C^1_{Fe}	35%	
C^2_{Fe}	65%	10%
C^3_{Fe}		90%

(10) and (11) spots of 1 ML Fe/Pd(001) are shown with solid lines. For the (10) spot, two remarkable intensity maxima appear around 68 and 136 eV and several peaks are observed in the energy range of 50–310 eV. On the other hand, for the (11) spot, four intensity maxima appear in the energy range of 70–400 eV. The calculated I-V curves with Fe-Pd intermixing reproduce the experimental results for both (10) and (11) spots well, as denoted with dashed lines. Thus, the minimum R factor ($R_{\text{P}} = 0.32$) and the error ($\delta R_{\text{P}} = 0.08$) for the interface atomic structure were found, as shown in Fig. 3(c). The most probable composition of Fe is 35% in the surface (S1) layer and 65% in the subsurface (S2) layer, which indicates a sizable amount of intermixing at the Fe-Pd interface. A value of $R_{\text{P}} = 0.32$ is acceptable for this kind of random surface alloy.[39] Note that the variation of the lattice parameters without intermixing is insufficient to find a reliable R_{P}. The relative interlayer relaxation for 1 ML Fe/Pd(001) is listed in Table I. The resultant values for the Fe composition are similar to those previously reported by Lee *et al.* ($35 \pm 15\%$ in the S1 layer and $90^{+10}_{-15}\%$ in the S2 layer).[16]

The interface atomic structure of the 1 ML Pd-capped Fe/Pd(001), which can be regarded as the thinnest case of the $L1_0$ structure, was also investigated. The observed I-V curves (solid lines) were found to be markedly different from those without Pd capping. For the (10) spot, the intensity ratio of the two peaks around 68 and 136 eV is interchanged with respect to those for 1 ML Fe/Pd(001). For the (11) spot, two peaks around 250 and 358 eV are predominant, while the peaks below 200 eV are suppressed compared to those for 1 ML Fe/Pd(001). At first, the calculated I-V spectra were obtained under the assumption that intermixing occurs in only three layers (S1, S2, and S3) and without temperature correction due to computational restrictions. However, no sizable amount of intermixing between the Fe and the Pd overlayer was found. Therefore, a pure Pd overlayer was assumed in the calculation when temperature correction was taken into account. This assumption can be justified by the fact that Pd has a lower surface free energy (2.04 J/m^2) than that of Fe (2.94 J/m^2).[40] The sharp LEED patterns after Pd deposition also support this assumption [see Figs. 2(d) and 2(e)] because surface intermixing could cause diffuse LEED spots and enhance the background intensity, as is observed in Figs. 2(b) and 2(c). $R_{\text{P}} = 0.31$ and $\delta R_{\text{P}} = 0.08$ for the interface atomic structure shown in Fig. 3(d). The Fe composition of the S2 and S3 layers is 10% and 90%, respectively, as shown in Table I. The surface interlayer relaxation d_{12} is expanded as compared to d_{bulk} in Pd/Fe/Pd(001). On the other hand, the interlayer distances around the Fe-rich layer (S3) d_{23} and d_{34} are strongly contracted with respect to d_{bulk}.

The difference of the degree of intermixing between bare Fe/Pd(001) and the Pd-capped Fe/Pd(001) is worthy of discussion. There are several possible reasons for this difference: (i) Pd capping stimulates Fe-Pd intermixing, (ii) fcc Pd is known to be a hydrogen storage material and hydrogen saturation of the substrate modifies interlayer distances, thus changing the degree of intermixing, and/or (iii) subtle substrate temperature and deposition rate variations result in differences in the degree of intermixing. Meyerheim *et al.* reported that intermixing in Fe/Pd(001) occurs at 330 K and no alloying takes place at 300 K.[17] In the present results, intermixing occurs at 310 K (RT for the present experiment); however, it cannot be excluded that the critical temperature for the onset of intermixing could be located in the narrow temperature window between 300 and 310 K. With this Pd/Fe/Pd(001), an almost perfect Pd-sandwiched Fe monolayer has been successfully fabricated. By clarifying the growth mechanism, it brings about the opportunity to fabricate the self-assembled Pd/Fe/Pd sandwiched monatomic structure.

B. Magnetic properties

An attempt to clarify the magnetic anisotropy of Fe monatomic films on Pd(001) without and with a Pd capping layer was made by measuring the ESMH curves and the angle-dependent XMCD spectra of the remanent magnetization. Figure 4 shows the Fe L_3 edge ESMH curves for Fe/Pd(001) and Pd/Fe/Pd(001) measured at 89 K. The normalization

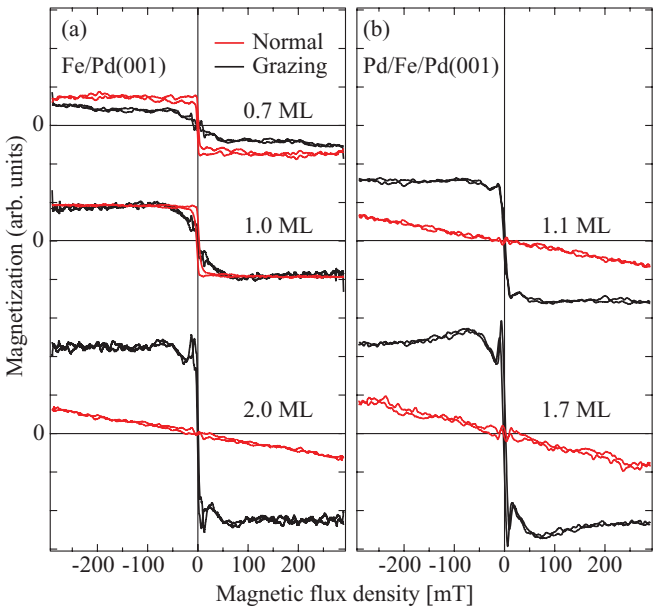

FIG. 4. (Color online) The Fe L_3 edge ESMH curves for (a) t ML Fe/Pd(001) ($t = 0.7, 1.0, 2.0$) and (b) 1 ML Pd/t ML Fe/Pd(001) ($t = 1.1, 1.7$) measured at 89 K. Red and black lines indicate the ESMH curves measured at normal (0°) and grazing (75°) incidence, respectively.

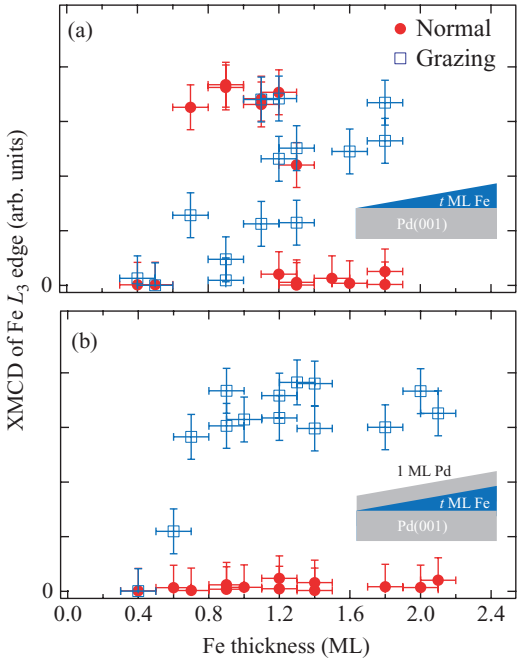

FIG. 5. (Color online) Fe thickness dependence of the Fe L_3 XMCD intensity of (a) t ML Fe/Pd(001) ($t = 0.4$–1.8) and (b) 1 ML Pd/t ML Fe/Pd(001) ($t = 0.4$–2.1) in remanent magnetization. Filled circles and open squares denote the XMCD intensity measured at normal (0°) and grazing (45°) incidence, which reflects the perpendicular and the in-plane magnetization, respectively.

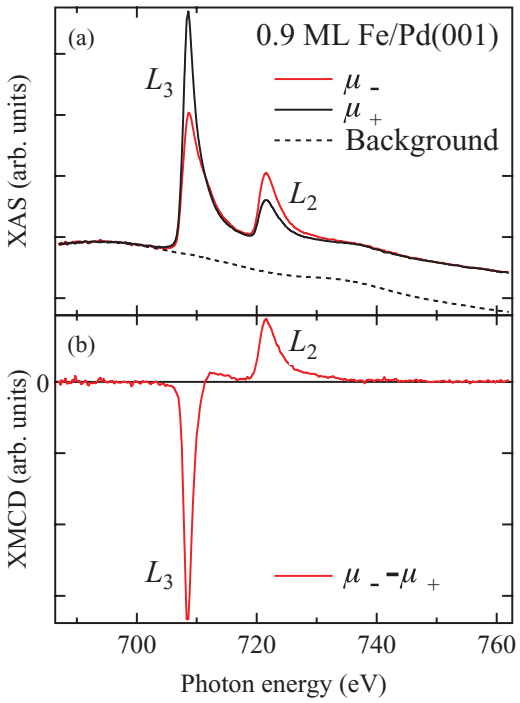

FIG. 6. (Color online) (a) XAS and (b) XMCD spectra at the Fe $L_{2,3}$ edges of 0.9 ML Fe/Pd(001) acquired under a perpendicular magnetic field of 1.3 T, with the light incidence angle normal to the surface. (a) Black and red solid lines represent the absorption spectra for different magnetization directions (μ_+, μ_-). Black dashed line represents the background signal contributed from the clean Pd substrate. (b) Red solid line represents the XMCD spectrum ($\mu_- - \mu_+$).

procedure introduced by Goering *et al*. was used to remove the background signal.[41] The spikes observed in the ESMH curves around zero magnetic field are extrinsic, but originate from the return of the photoelectron to the sample. The easy magnetization axis was found to be perpendicular to the surface for the 0.7 and 1.0 ML Fe/Pd(001) samples and is in-plane at 2.0 ML, as shown in Fig. 4(a). In Fig. 4(b), on the other hand, the easy axis is always oriented along the in-plane direction for Pd/Fe/Pd(001). Figure 5 shows the thickness dependence of the Fe L_3 edge XMCD intensity obtained under remanence magnetization conditions (0 T). As shown in Fig. 5(a), the perpendicular magnetization appears in the low coverage region ($t \leqslant 1.2$ ML) and abruptly disappears above 1.2 ML for Fe/Pd(001). Conversely, as shown in Fig. 5(b), the in-plane magnetization appears throughout the whole Fe thickness range for Pd/Fe/Pd(001). Thus, the Pd overlayer obviously affects the magnetic anisotropy of Fe. The negligible XMCD intensity below 0.5 ML is considered to be due to the disappearance of the ferromagnetic order due to a reduced Curie temperature.

In order to reveal the relationship between the magnetic anisotropy and the magnetic moment, the Fe thickness dependence of the XMCD spectra was measured, and the magnetic moments were evaluated with the use of magneto-optical sum rules.[43,44] Figure 6 shows typical Fe $L_{2,3}$ edge XAS and XMCD spectra for 0.9 ML Fe/Pd(001) acquired under a perpendicular magnetic field of 1.3 T. Two white lines are found at photon energies of 709 and 722 eV corresponding to the L_3 and L_2 edges. A broad hump on the higher-energy side of the L_2 peak originates from the Pd substrate without any dichroic signals. In Fig. 6(b), a clear XMCD signal appears with negative and positive signs at the L_3 and L_2 edges, respectively. The background signal from the Pd substrate has been subtracted from the XAS spectra [Fig. 6(a)]. For the sum-rule analysis, the Fe 3d hole number was assumed to be 3.39.[42] The magnetic dipole moment (m_T) is effectively included in m_{spin}^{eff} (which equals $m_{spin} + 7m_T$). Figures 7(a) and 7(b) show the Fe thickness dependence of the Fe 3d spin (m_{spin}^{eff}) and orbital (m_{orb}) magnetic moments for t ML Fe/Pd(001) and 1 ML Pd/t ML Fe/Pd(001), respectively, where t represents the film thickness [$t = 0.1$–3.5 for t ML Fe/Pd(001) and $t = 0.1$–1.7 for 1 ML Pd/t ML Fe/Pd(001)]. Previous results by Le Cann *et al*.[20] are also shown for comparison (see the insets in Fig. 7). Note that the overall trends in m_{spin}^{eff} and m_{orb} with Fe thickness are similar. The effective spin magnetic moment and the perpendicular component of m_{orb} near 1 ML ($m_{spin}^{eff} = 2.38\mu_B$ and $m_{orb} = 0.123\mu_B$) are larger than those of bulk bcc Fe ($1.98\mu_B$ and $0.085\mu_B$, respectively).[42] However, there is no significant difference between the values of m_{spin}^{eff} and m_{orb} for samples with and without the Pd overlayer. The rapid decrease of m_{spin}^{eff} and m_{orb} below 0.5 ML might be due to the absence of ferromagnetic order as a result of a reduced Curie temperature. Decreased values of m_{spin}^{eff} and m_{orb} above 2 ML likely originate from the presence of in-plane magnetic anisotropy. Therefore, the perpendicular magnetic field of 1.3 T may not be strong enough to saturate the magnetization. Another possibility is that the decrease comes from an intrinsic reduction of the magnetic moment toward

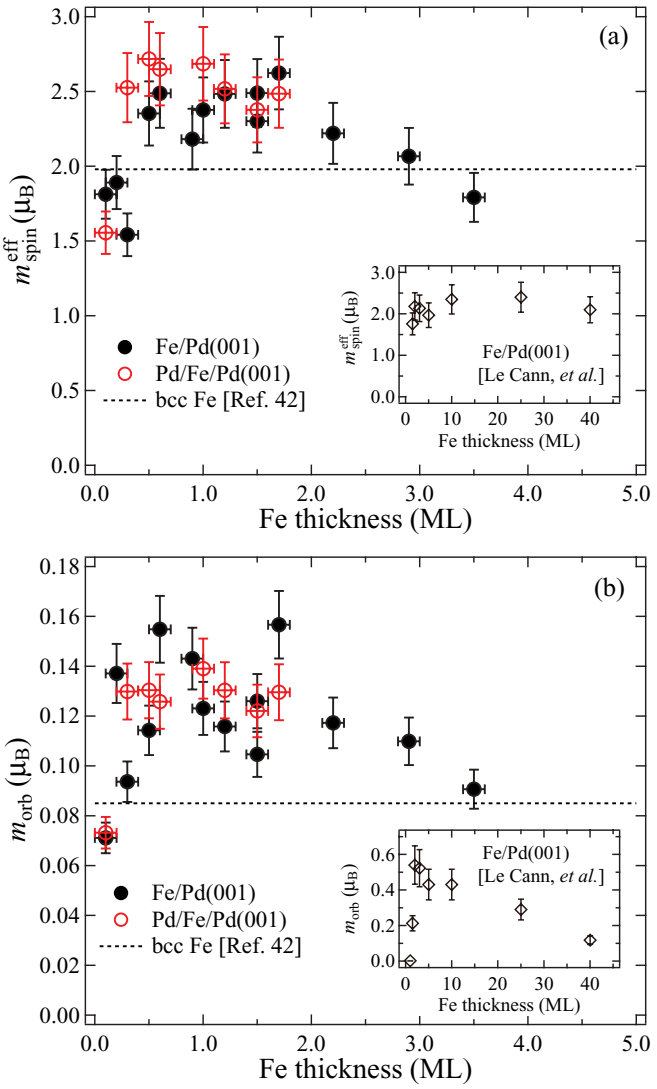

FIG. 7. (Color online) Fe 3*d* (a) spin magnetic moment (m^{eff}_{spin}) (μ_B) and (b) orbital magnetic moment (m_{orb}) (μ_B) of *t* ML Fe and 1 ML Pd/*t* ML Fe on Pd(001), respectively. Filled and open circles denote the values for *t* ML Fe/Pd(001) ($t = 0.1$–3.5) and 1 ML Pd/*t* ML Fe/Pd(001) ($t = 0.1$–1.7), respectively. Dashed line denotes the values for the bulk bcc Fe.[42] (Insets) Open diamonds denote the values for *t* ML Fe/Pd(001) ($t = 1$–40) from Ref. 20.

the bulk value. It seems that there is no special relationship between the magnetic moment and the magnetic anisotropy of Fe/Pd(001) and Pd/Fe/Pd(001) because the quantities m^{eff}_{spin} and m_{orb} are almost constant around the critical thickness for the SRT in Fe/Pd(001), with or without a Pd overlayer.

An attempt was also made to detect a magnetic signal from the Pd substrate. Figure 8 shows the XAS and XMCD spectra of Fe/Pd(001) at the Pd $M_{2,3}$ edges measured with a perpendicular magnetic field of 1.3 T. In Fig. 8(a), two white lines appear at photon energies of 529 and 556 eV corresponding to the M_3 and M_2 edges, respectively. Weak but finite intensity differences appear at the M_2 and M_3 edges for different magnetization directions. The Fe thickness dependence of the XMCD spectra at the Pd $M_{2,3}$ edges is shown in Fig. 8(b). A clear XMCD signal is observed at the Pd $M_{2,3}$ edges, which indicates the presence of induced magnetic

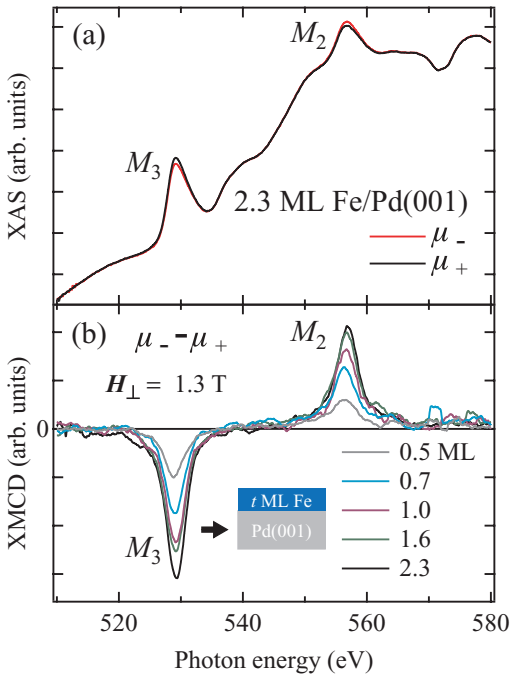

FIG. 8. (Color online) (a) Pd $M_{2,3}$ XAS spectra of 2.3 ML Fe/Pd(001) acquired under a perpendicular magnetic field of 1.3 T. Black and red (bright) solid lines represent the absorption spectra for different magnetization directions (μ_+, μ_-). (b) Pd $M_{2,3}$ XMCD spectra of *t* ML Fe/Pd(001) ($t = 0.5$–2.3). XMCD spectra are normalized by XAS M_3 peak intensity for each Fe thickness.

moments on the Pd atoms. The observation of the same polarity in the XMCD spectrum as that at the Fe $L_{2,3}$ edges suggests that the Fe and Pd magnetic moments are ferromagnetically coupled. Since the Pd $M_{2,3}$ XMCD is more pronounced with increased Fe coverage, it is concluded that the Pd 4*d* magnetic moment is induced mainly at the Fe-Pd interface.

C. First-principles calculation

In order to get more insight into the origin of the magnetic anisotropy from the standpoint of electronic structure, a first-principles calculation was performed. Four slab models were examined. The 1 ML Fe/Pd(001) and 2 ML Fe/Pd(001) slabs were considered here to demonstrate the Fe thickness dependence of the magnetic anisotropy. A 1 ML Pd/1 ML Fe/Pd(001) slab was studied as an ideal Pd/Fe bilayer film. And finally, a 2 ML Pd/1 ML Fe/Pd(001) slab was assumed to be analogous to the actual structure of 1 ML Pd-capped 1 ML Fe/Pd(001) as determined by the LEED *I*-*V* experiments [see Fig. 3(d)]. Here, the Pd atoms contained in the slab are distinguished with the following notations; the capping layers Pd(c1) and Pd(c2), the substrate layer adjoining the Fe layer Pd(s1), and the second and third next-adjoining layer Pd(s2) and Pd(s3). The optimized interlayer distance in each slab is listed in Table II. All Pd-Pd interlayer distances are relaxed compared to that of the bulk fcc Pd (1.945 Å). The interlayer distances around the Fe layer [Pd(c1)-Fe and Fe-Pd(s1)] are similar to those in Fe/Pd(001) and Pd/Fe/Pd(001) except for a slightly longer Fe-Pd(s1) distance in 1 ML Pd/1 ML Fe/Pd(001).

TABLE II. Optimized interlayer distances (Å) in Fe(1 ML)/Pd(001) and Pd(1 and 2 ML)/Fe/Pd(001) in the calculation. c1 and c2 denote Pd overlayers that are nearest and next nearest, respectively, to the Fe layer for Pd(1 and 2 ML)/Fe/Pd(001). s1, s2, and s3 denote the underlayer (substrate) Pd that is nearest, next, and second next nearest, respectively.

	Layer distance (Å)				
	Pd(c2)-Pd(c1)	Pd(c1)-Fe	Fe-Pd(s1)	Pd(s1)-Pd(s2)	Pd(s2)-Pd(s3)
1 ML Fe/Pd(001)			1.76	2.07	2.02
1 ML Pd/1 ML Fe/Pd(001)		1.76	1.79	2.06	2.02
2 ML Pd/1 ML Fe/Pd(001)	2.00	1.75	1.76	2.06	2.02

Magnetic anisotropy energies (MAEs) in each slab are summarized in Table III. The MAE caused by the spin-orbit interaction (E_{SO}) is positive in 1 and 2 ML Fe/Pd(001), as well as 2 ML Pd/1 ML Fe/Pd(001). On the other hand, E_{SO} is negative in 1 ML Pd/1 ML Fe/Pd(001). The magnetic dipole-dipole interaction energy (E_D) for 2 ML Fe/Pd(001), which prefers in-plane magnetic anisotropy, is twice as large as that in the 1 ML Fe/Pd(001) due to the doubled Fe magnetic moment in the slab because the main component of E_D comes from the large spin magnetic moment of Fe (see Table IV). As a result, the net magnetic anisotropy energy $E = E_{SO} + E_D$ is positive in 1 ML Fe and 2 ML Pd/1 ML Fe and negative in 2 ML Fe and 1 ML Pd/1 ML Fe. This means that PMA is preferred for 1 ML Fe and 2 ML Pd/1 ML Fe, while in-plane magnetic anisotropy is stabilized for 2 ML Fe and 1 ML Pd/1 ML Fe. The theoretical PMA is inconsistent with the experimental result for 1 ML Pd-capped 1 ML Fe/Pd(001), which prefers in-plane magnetization, and with actual interface structure as shown in Fig. 3(d).

The calculated spin (m_{spin}) and orbital (m_{orb}) magnetic moments in each system are compiled in Table IV. Of note is that m_{spin} does not depend on the magnetization direction, while m_{orb} shows a marked difference along two magnetization directions. In particular, m_{orb} for the 1 ML Fe/Pd(001) is enhanced by about 15% along the [001] direction as opposed to the [100] direction. The induced spin magnetic moment of about 0.32–0.34μ_B for the interface Pd in the calculation qualitatively explains the experimental Pd $M_{2,3}$ XMCD spectra in Fig. 8(b). The spin moments at the Pd(c1) and Pd(s1) layers adjoining to the Fe layer are obviously enhanced compared to those at the next-adjoining layers Pd(c2) and Pd(s2). The orbital magnetic moment is enhanced in the surface Fe [in the 1 ML Fe/Pd(001) system] compared to that of the embedded Fe [in the 1 and 2 ML Pd/1 ML Fe/Pd(001) systems], which is due to reduced coordination at the surface.

TABLE III. Magnetic anisotropy energy (MAE) (meV/Fe atom) from spin-orbit interaction (E_{SO}), from magnetic dipole-dipole interaction (E_D), and their net MAE (E) in Fe(1 and 2 ML)/Pd(001) and Pd(1 and 2 ML)/Fe/Pd(001).

	MAE (meV/Fe atom)		
	E_{SO}	E_D	E
1 ML Fe/Pd(001)	0.24	−0.20	0.05
2 ML Fe/Pd(001)	0.34	−0.39	−0.05
1 ML Pd/1 ML Fe/Pd(001)	−0.20	−0.20	−0.41
2 ML Pd/1 ML Fe/Pd(001)	0.28	−0.20	0.08

Figure 9 shows the calculated electronic band dispersions of 1 ML Fe/Pd(001) [Figs. 9(a)–9(c)], 1 ML Pd/1 ML Fe/Pd(001) [Figs. 9(d)–9(f)], and 2 ML Pd/1 ML Fe/Pd(001) [Figs. 9(g)–9(i)]. The Fe 3d orbital components ($d_{3z^2-r^2}$, d_{xz}, d_{yz}, d_{xy}, and $d_{x^2-y^2}$) are highlighted by markers. Next, each Fe 3d orbital component is compared between the three systems. First, the $3d_{3z^2-r^2}$ orbital is examined [Figs. 9(a), 9(d), and 9(g)]. The most significant difference appears around the $\bar{X}$ point near the Fermi energy. Here, the two $3d_{3z^2-r^2}$ bands are split into occupied and unoccupied states for 1 ML Fe/Pd(001) [Fig. 9(a)] and for 2 ML Pd/1 ML Fe/Pd(001) [Fig. 9(g)], while both bands are occupied for 1 ML Pd/1 ML Fe/Pd(001) [Fig. 9(d)]. In Figs. 9(b), 9(e), and 9(h), a higher-energy shift for the Fe $3d_{xz}$ and $3d_{yz}$ band dispersions is found around $\bar{M}$ upon 1 or 2 ML Pd capping. In Figs. 9(c), 9(f), and 9(i), a similar energy shift around $\bar{M}$ is found for the Fe $3d_{xy}$ band. These energy shifts in the Fe 3d orbitals are attributed to the charge transfer from Fe to Pd by the Fe 3d–Pd 4d orbital hybridization. In addition, the occupied states of the Fe $3d_{xz}$ and $3d_{yz}$ between $\bar{X}$-$\bar{\Gamma}$ are influenced by Pd capping [Figs. 9(b), 9(e), and 9(h)]. In particular, the narrow Fe $3d_{yz}$ bands at the $\bar{X}$ point around −0.3 eV in 1 ML Fe/Pd(001) are substantially modified upon Pd capping because these orbitals are elongated in the direction of the Pd atom and can easily hybridize with the Pd atomic orbitals.

D. Discussion

In discussing the relationship between the interface atomic structures and the magnetic anisotropy of monatomic Fe and Pd/Fe on Pd(001), the focus is placed upon 1 ML Fe/Pd(001) and 1 ML Pd-capped 1 ML Fe/Pd(001) (2 ML Pd/1 ML Fe/Pd(001) in the calculation), because their magnetic properties and atomic structures were established above. As for the magnetic anisotropy shown in Figs. 4 and 5, the PMA in Fe/Pd(001) is observed to appear only below a critical Fe thickness and the easy axis is changed to the in-plane direction above 1.2 ML. On the other hand, in the presence of the Pd overlayer, it exhibits in-plane magnetic anisotropy below 2 ML. Thus it is revealed that perpendicular magnetization is more stable for 1 ML Fe/Pd(001), while in-plane magnetization is favored in 2 ML Fe/Pd(001) and 1 ML Pd-capped Fe/Pd(001). However, no PMA was observed in the previous SMOKE experiment on Fe film grown on Pd(001) at RT. On the contrary, PMA has been observed in Fe/Pd(001) grown at low temperature.[18,19] As argued in several previous studies on the interface structures of Fe/Pd(001), it is considered that intermixing between Fe and

TABLE IV. Spin (m_{spin}) and orbital (m_{orb}) magnetic moments in units of μ_B on Fe and Pd atoms in 1 ML Fe/Pd(001) and Pd(1 and 2 ML)/Fe/Pd(001) when magnetized perpendicular ([001]) and parallel ([100]) to the surface.

	Magnetization direction	m_{spin} (μ_B)					m_{orb} (μ_B)				
		Pd(c2)	Pd(c1)	Fe	Pd(s1)	Pd(s2)	Pd(c2)	Pd(c1)	Fe	Pd(s1)	Pd(s2)
1 ML Fe/Pd(001)	[001]			3.260	0.316	0.185			0.080	0.025	0.024
	[100]			3.260	0.317	0.187			0.068	0.032	0.018
1 ML Pd/1 ML Fe/Pd(001)	[001]		0.326	3.266	0.344	0.189		0.027	0.050	0.029	0.021
	[100]		0.328	3.266	0.344	0.189		0.040	0.045	0.034	0.020
2 ML Pd/1 ML Fe/Pd(001)	[001]	0.098	0.333	3.250	0.338	0.189	0.011	0.027	0.059	0.027	0.020
	[100]	0.097	0.333	3.250	0.338	0.188	0.014	0.030	0.053	0.032	0.018

Pd atoms at the interface significantly affects the magnetic anisotropy. Here, the interface atomic structures of 1 ML Fe/Pd(001) and 1 ML Pd-capped 1 ML Fe/Pd(001) have been determined, and a sizable amount of interlayer mixing between Fe and Pd has been found to occur at RT. In 1 ML Fe/Pd(001), the interlayer distances around the Fe-rich layer d_{12} and d_{23} are 1.86 and 1.81 Å, respectively (Fig. 3). These values are similar to the interlayer distances in an $L1_0$-ordered FePd alloy (1.86 Å).[45] Therefore, by considering intermixing and interlayer distances, it is concluded that an $L1_0$-like ultrathin film structure and PMA are realized in 1 ML Fe/Pd(001).

The magnetocrystalline anisotropy energy E_{SO} is known to be proportional to the difference between the perpendicular and parallel components of the orbital magnetic moment ($m_{orb}^{\perp} - m_{orb}^{\parallel}$).[46] Note that this relationship is found to be applicable to pure magnetic films with a large exchange splitting,[47] but it fails to explain the magnetic anisotropy of compounds.[48] Although an extended formula for this relationship has also been derived,[49] it seems too complicated

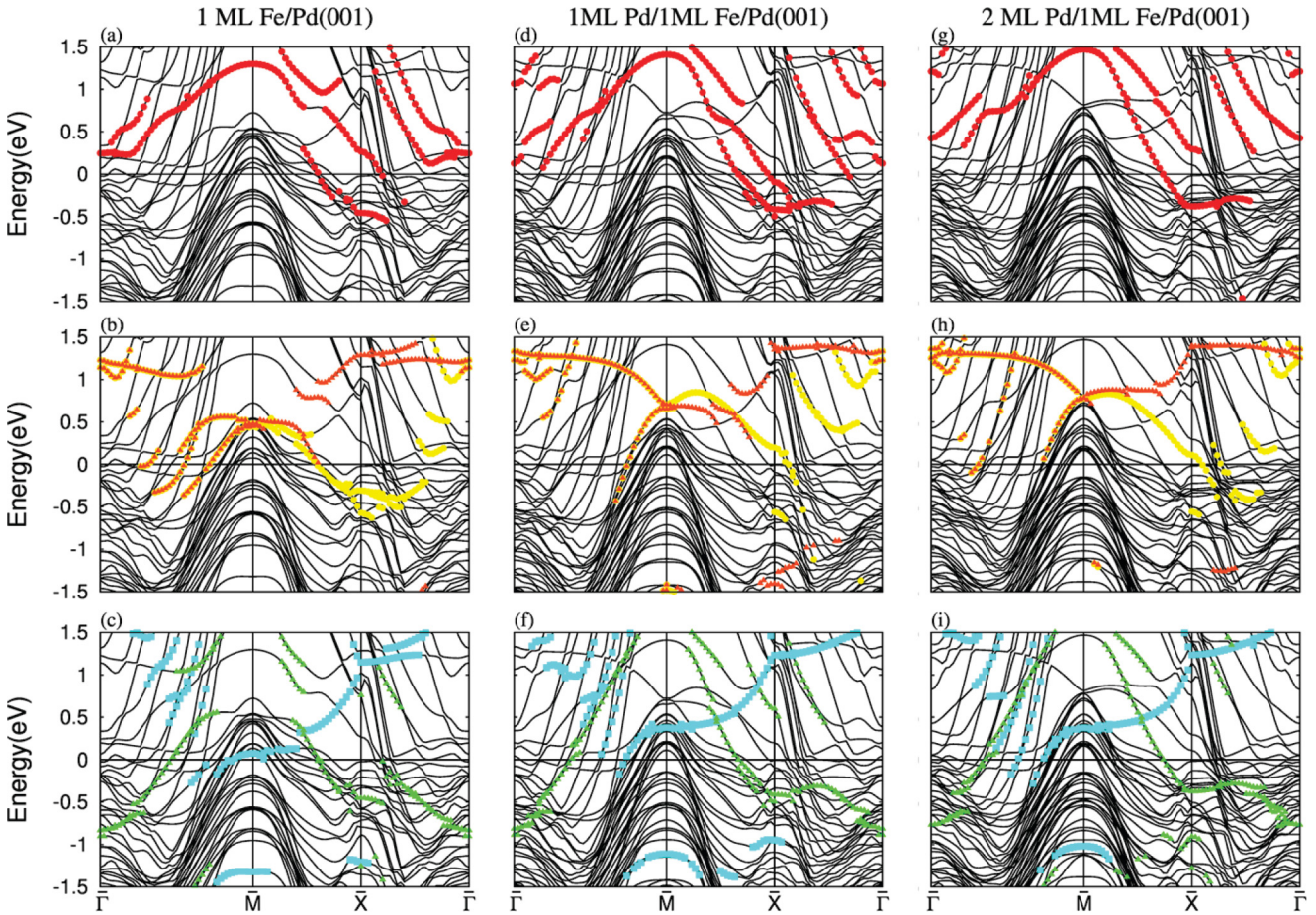

FIG. 9. (Color online) Electronic band dispersions of (a)–(c) 1 ML Fe/Pd(001), (d)–(f) 1 ML Pd/1 ML Fe/Pd(001), and (g)–(i) 2 ML Pd/1 ML Fe/Pd(001). Fermi energy corresponds to 0 eV. The magnetization direction is along [001]. The Fe orbital local components of $d_{3z^2-r^2}$, d_{xz}, d_{yz}, d_{xy}, and $d_{x^2-y^2}$ for minority spin states are marked as red circles, orange triangles, yellow circles, blue squares, and green triangles, respectively.

to be applied. Thus we consider the simplest model $E_{SO} \propto m^{\perp}_{orb} - m^{\parallel}_{orb}$. The same size of orbital moment was observed for bare and 1 ML Pd-capped Fe/Pd(001) below 1.2 ML [see Fig. 7(b)] in contrast to the difference of the magnetic anisotropy as shown in Figs. 4 and 5. In the present study, only $m^{\perp}_{orb}$ is obtained due to the limitation of the experimental configuration. Therefore, we speculate that the difference of the magnetic anisotropy may come from the difference in $m^{\parallel}_{orb}$. From the calculated results listed in Table IV, the induced magnetic moments at Pd atoms seem to play an important role in the magnetic anisotropy because the difference of m_{orb} at the interface Pd [Pd(c1) and Pd(s1)] with two magnetization directions is comparable to that at Fe. In addition, the sign in the difference of m_{orb} at Pd atoms is opposite to that at Fe. Experimental quantification of the magnetic moment at the interface Pd would help to unveil the origin of the magnetic anisotropy. By the way, the origin of the same size of $m^{\perp}_{orb}$ [Fig. 7(b)] may be attributed to the intermixed interface structure which results from the unchanged Fe local coordinates with or without the Pd capping. This speculation is theoretically supported by the obviously enhanced m_{orb} for the surface Fe atoms compared to the embedded Fe atoms as shown in Table IV.

The chemical order (CO) of the alloy affects its magnetic anisotropy. The degree of the CO is defined as $d_{CO} = |n_{Fe} - n_{Pd}|$, where n_{Fe} and n_{Pd} are Fe-atom occupations at the correct Fe and Pd sites in the $L1_0$ structure, respectively. By following this definition, $d_{CO} = 0.3$ in Fe/Pd(001) and $d_{CO} = 0.8$ in Pd/Fe/Pd(001) here. Kamp *et al.* reported a correlation between the magnetic anisotropy and the CO in FePd alloy films on MgO(001).[10] They obtained an increase in the Fe 3*d* orbital magnetic moment with increasing d_{CO}. In the present case, however, no remarkable difference in Fe 3*d* orbital moments is found between Fe/Pd(001) and Pd/Fe/Pd(001) as shown in Fig. 7(b), although the d_{CO} differences are noticeable. This discrepancy may come from the different film thickness; i.e., 300 Å in Ref. 10 and monatomic film in the present study. This indicates that the CO of the alloy is not particularly important in determining the orbital magnetic moment in the monatomic regime. It also seems that the d_{CO} is not the crucial parameter in determining the magnetic anisotropy in the monatomic regime because the PMA is stable in the $L1_0$-like structure with a low d_{CO}. It is likely that local hybridization between the Fe 3*d* and Pd 4*d* orbitals is more important than long-range order of the crystalline structure in the exhibition of uniaxial magnetic anisotropy by the $L1_0$-like FePd monatomic film.

The relationship between the tetragonal distortion and the magnetic anisotropy is discussed next.[50] In an Fe/Pd system, the lattice constants of fcc Pd and fcc Fe are 3.89 and 3.59 Å, respectively.[14] In order to maintain the atomic volume, the out-of-plane lattice constant of the Fe film contracts. Then, a face-centered-tetragonal (fct) FePd alloy appears on the Pd(001) surface, as shown in Figs. 3(c) and 3(d). In 1 ML Pd-capped 1 ML Fe/Pd(001), the interlayer distances around the Fe-rich layer, d_{23} and d_{34}, are contracted by about 0.1 Å as compared to those in 1 ML Fe/Pd(001). Then, the c/a ratio in 1 ML Pd-capped 1 ML Fe/Pd(001) becomes smaller than that in 1 ML Fe/Pd(001). The reduction of the c/a ratio corresponds to the difference in the easy magnetization direction as shown in Figs. 4 and 5. In bulk $L1_0$ FePd, a reduction in MAE is also cooperating with the decrease in the c/a ratio from $c/a = 1$.[51]

The spin reorientation transition in Fe/Pd(001) is explained by the large E_D with increasing Fe thickness, because the E_D in 2 ML Fe/Pd(001) is twice as large as that in 1 ML Fe/Pd(001), as shown in Table III. The perpendicular magnetization in the $L1_0$-like structure of 1 ML Fe/Pd(001) is broken up with the dominance of the dipole energy due to additional Fe magnetic moments.

Finally, the experimental and theoretical results of the Pd/Fe/Pd(001) system are compared with those of the Pt/Fe/Pt(001) system. Imada *et al.* reported that m_{spin} is about $2.4\mu_B$/Fe for 1 ML Fe sandwiched by the Pt layers under 1.4 T at 90 K.[6] This value is comparable to the present $m^{eff}_{spin} \sim 2.5\mu_B$ for Fe/Pd(001) and Pd/Fe/Pd(001) around an Fe thickness of 1 ML. Of note is that several points are similar in the calculated m_{spin} and m_{orb} of the Fe/Pd system and the Fe/Pt system.[7] The m_{spin} of the capped Fe is slightly enhanced compared to the bare Fe in both systems. This is likely due to enhanced hybridization between the Fe 3*d* and Pd 4*d* or Pt 5*d* orbitals in the sandwich systems. The value of m_{orb} of bare Fe is larger than that of the capped Fe in both systems, which might be due to the reduced atomic coordination for the bare Fe film.

IV. CONCLUSIONS

In conclusion, the interface atomic structures and magnetic anisotropy of Fe and Pd/Fe monatomic films on Pd(001) were investigated with a combination of LEED *I*-*V*, XMCD, and first-principles calculations. It was revealed that intermixing between Fe and the Pd substrate occurs at RT, and that the interlayer distances around the Fe-rich layer contract with the Pd overlayer. Fe/Pd(001) was found to exhibit perpendicular magnetization, turning to in-plane with increasing Fe thickness, and the in-plane magnetization was found to be persistently stable in Pd/Fe/Pd(001). Quantitative XMCD analysis revealed that the Fe 3*d* spin and orbital magnetic moments are enhanced in both bare Fe and Pd-capped Fe around 1 ML, as compared to bulk Fe. An $L1_0$-like Fe-Pd interface structure is realized in 1 ML Fe/Pd(001), and it exhibits PMA, which indicates that the uniaxial magnetic anisotropy of the $L1_0$-ordered alloy still exists in the ultrathin limit. On the other hand, the disappearance of the PMA in fcc-like Pd/Fe/Pd(001) indicates that tetragonal distortion of the crystal structure is key to the exhibition of PMA in these Fe/Pd systems.

ACKNOWLEDGMENTS

Experiments were performed at HSRC under the approval of the Proposal Assessing Committee as Proposal No. 08-A-14. The authors thank the Supercomputer Center, Institute for Solid State Physics, the University of Tokyo, and Information Media Center, Hiroshima University for the use of their facilities. This work is supported by research fellowships of the Japan Society for the Promotion of Science for Young Scientists (No. 21·2032).

*Author to whom all correspondence should be addressed: tetsuro-ueno@hiroshima-u.ac.jp

[1] M. Wuttig, B. Feldmann, and T. Flores, Surf. Sci. **331**, 659 (1995).
[2] J. Shen and J. Kirschner, Surf. Sci. **500**, 300 (2002).
[3] W. B. Zeper, F. J. A. M. Greidanus, P. F. Carcia, and C. R. Fincher, J. Appl. Phys. **65**, 4971 (1989).
[4] M. N. Baibich, J. M. Broto, A. Fert, F. Nguyen Van Dau, F. Petroff, P. Etienne, G. Creuzet, A. Friederich, and J. Chazelas, Phys. Rev. Lett. **61**, 2472 (1988).
[5] G. Binasch, P. Grünberg, F. Saurenbach, and W. Zinn, Phys. Rev. B **39**, 4828 (1989).
[6] S. Imada, A. Yamasaki, S. Suga, T. Shima, and K. Takanashi, Appl. Phys. Lett. **90**, 132507 (2007).
[7] M. Tsujikawa, A. Hosokawa, and T. Oda, Phys. Rev. B **77**, 054413 (2008).
[8] H. Chen, N. E. Brener, and J. Callaway, Phys. Rev. B **40**, 1443 (1989).
[9] V. Gehanno, A. Marty, B. Gilles, and Y. Samson, Phys. Rev. B **55**, 12552 (1997).
[10] P. Kamp, A. Marty, B. Gilles, R. Hoffmann, S. Marchesini, M. Belakhovsky, C. Boeglin, H. A. Dürr, S. S. Dhesi, G. van der Laan, and A. Rogalev, Phys. Rev. B **59**, 1105 (1999).
[11] M. Weisheit, S. Fähler, A. Marty, Y. Souche, C. Poinsignon, and D. Givord, Science **315**, 349 (2007).
[12] S. Haraguchi, M. Tsujikawa, J. Gotou, and T. Oda, J. Phys. D **44**, 064005 (2011).
[13] J. Quinn, Y. S. Li, H. Li, D. Tian, F. Jona, and P. M. Marcus, Phys. Rev. B **43**, 3959 (1991).
[14] X. F. Jin, J. Barthel, J. Shen, S. S. Manoharan, and J. Kirschner, Phys. Rev. B **60**, 11809 (1999).
[15] C. Boeglin, H. Bulou, J. Hommet, X. Le Cann, H. Magnan, P. Le Fèvre, and D. Chandesris, Phys. Rev. B **60**, 4220 (1999).
[16] S.-K. Lee, J.-S. Kim, B. Kim, Y. Cha, W. K. Han, H. G. Min, J. Seo, and S. C. Hong, Phys. Rev. B **65**, 014423 (2001).
[17] H. L. Meyerheim, R. Popescu, and J. Kirschner, Phys. Rev. B **73**, 245432 (2006).
[18] C. Liu and S. D. Bader, Phys. Rev. B **44**, 2205 (1991).
[19] C. Liu and S. D. Bader, J. Magn. Magn. Mater. **93**, 307 (1991).
[20] X. Le Cann, C. Boeglin, B. Carrière, and K. Hricovini, Phys. Rev. B **54**, 373 (1996).
[21] X. Le Cann, C. Boeglin, K. Hricovini, and B. Carrière, Thin Solid Films **275**, 95 (1996).
[22] J. Vogel, A. Fontaine, V. Cros, F. Petroff, J.-P. Kappler, G. Krill, A. Rogalev, and J. Goulon, J. Magn. Magn. Mater. **165**, 96 (1997).
[23] V. Cros, F. Petroff, J. Vogel, A. Fontaine, J. L. Menéndez, A. Cebollada, W. Grange, J.-P. Kappler, M. Finazzi, and N. B. Brookes, Europhys. Lett. **49**, 807 (2000).
[24] T. Ueno, M. Nagira, S. Tohoda, T. Tagashira, A. Kimura, M. Sawada, H. Namatame, and M. Taniguchi, e-J. Surf. Sci. Nanotech. **6**, 246 (2008).
[25] A. Barbieri and M. A. van Hove (private communication) (http://www.ap.cityu.edu.hk/personal-website/Van-Hove.htm).
[26] J. B. Pendry, J. Phys. C **13**, 937 (1980).
[27] F. Jona, K. O. Legg, H. D. Shih, D. W. Jepsen, and P. M. Marcus, Phys. Rev. Lett. **40**, 1466 (1978).
[28] V. Blum, C. Rath, S. Müller, L. Hammer, K. Heinz, J. M. García, J. E. Ortega, J. E. Prieto, O. S. Hernán, J. M. Gallego, A. L. Vázquez de Parga, and R. Miranda, Phys. Rev. B **59**, 15966 (1999).
[29] M. Sawada, K. Yaji, M. Nagira, A. Kimura, H. Namatame, and M. Taniguchi, in *9th International Conference on Synchrotron Radiation Instrumentation*, AIP Conf. Proc. No. 879 (AIP, New York, 2007), p. 551.
[30] M. Sawada, T. Ueno, T. Tagashira, H. Namatame, and M. Taniguchi, in *10th International Conference on Synchrotron Radiation Instrumentation*, AIP Conf. Proc. No. 1234 (AIP, New York, 2010), p. 939.
[31] J. P. Perdew, J. A. Chevary, S. H. Vosko, K. A. Jackson, M. R. Pederson, D. J. Singh, and C. Fiolhais, Phys. Rev. B **46**, 6671 (1992).
[32] W. Kohn and L. J. Sham, Phys. Rev. **140**, A1133 (1965).
[33] T. Oda and A. Hosokawa, Phys. Rev. B **72**, 224428 (2005).
[34] T. Oda, A. Pasquarello, and R. Car, Phys. Rev. Lett. **80**, 3622 (1998).
[35] D. Vanderbilt, Phys. Rev. B **41**, 7892 (1990).
[36] K. Laasonen, A. Pasquarello, R. Car, C. Lee, and D. Vanderbilt, Phys. Rev. B **47**, 10142 (1993).
[37] L. Szunyogh, B. Újfalussy, and P. Weinberger, Phys. Rev. B **51**, 9552 (1995).
[38] H. J. Monkhorst and J. D. Pack, Phys. Rev. B **13**, 5188 (1976).
[39] A. Atrei, U. Bardi, M. Galeotti, G. Rovida, M. Torrini, and E. Zanazzi, Surf. Sci. **339**, 323 (1995).
[40] L. Z. Mezey and J. Giber, Jpn. J. Appl. Phys. **21**, 1569 (1982).
[41] E. Goering, A. Fuss, W. Weber, J. Will, and G. Schütz, J. Appl. Phys. **88**, 5920 (2000).
[42] C. T. Chen, Y. U. Idzerda, H.-J. Lin, N. V. Smith, G. Meigs, E. Chaban, G. H. Ho, E. Pellegrin, and F. Sette, Phys. Rev. Lett. **75**, 152 (1995).
[43] B. T. Thole, P. Carra, F. Sette, and G. van der Laan, Phys. Rev. Lett. **68**, 1943 (1992).
[44] P. Carra, B. T. Thole, M. Altarelli, and X. D. Wang, Phys. Rev. Lett. **70**, 694 (1993).
[45] D. Halley, A. Marty, P. Bayle-Guillemaud, B. Gilles, J. P. Attane, and Y. Samson, Phys. Rev. B **70**, 174438 (2004).
[46] P. Bruno, Phys. Rev. B **39**, 865 (1989).
[47] D. Weller, J. Stöhr, R. Nakajima, A. Carl, M. G. Samant, C. Chappert, R. Mégy, P. Beauvillain, P. Veillet, and G. A. Held, Phys. Rev. Lett. **75**, 3752 (1995).
[48] P. Ravindran, A. Kjekshus, H. Fjellvåg, P. James, L. Nordström, B. Johansson, and O. Eriksson, Phys. Rev. B **63**, 144409 (2001).
[49] G. van der Laan, J. Phys.: Condens. Matter **10**, 3239 (1998).
[50] T. Burkert, L. Nordström, O. Eriksson, and O. Heinonen, Phys. Rev. Lett. **93**, 027203 (2004).
[51] H. Shima, K. Oikawa, A. Fujita, K. Fukamichi, K. Ishida, and A. Sakuma, Phys. Rev. B **70**, 224408 (2004).